T. Matsuura, Y. Egashira, T. Nishio, Y. Matsumoto, M. Wada, S. Koike, Y. Furusawa, R. Kohno, S. Nishioka, S. Kameoka, K. Tuchihara, M. Kawashima, T. Ogino	Apparent absence of a proton beam dose rate effect and possible differences in RBE between Bragg peak and plateau	Med. Phys.	37(10)	5376-5381	2010
A. Miyatake, T. Nishio, T. Ogino, N. Saijo, H. Esumi, M. Uesaka	Measurement and verification of positron emitter nuclei generated at each treatment site by target nuclear fragment reactions in proton therapy	Med. Phys.	37(8)	4445-4455	2010
S. Yonai, Y. Kase, N. Matsufuji, T. Kanai, T. Nishio, M. Namba, W. Yamashita, H. Yamashita	Measurement of absorbed dose, quality factor, and dose equivalent in water phantom outside of the irradiation field in passive carbon-ion and proton radiotherapies	Med. Phys.	37(8)	4046-4055	2010
T. Nishio	Tendency of physical irradiation parameter and spec of device obtained from results of proton treatment planning	Jpn. J. Clin. Radiol.	55(7)	843-852	2010
K. Hotta, R. Kohno, Y. Takada, Y. Hara, R. Tansho, T. Himukai, S. Kameoka, T. Matsuura, T. Nishio, T. Ogino	Improved dose-calculation accuracy in proton treatment planning using a simplified Monte Carlo method verified with three-dimensional measurements in an anthropomorphic phantom	Phys. Med. Biol.	55	3545-3556	2010

M. Kawashima, R. Kohno, K. Nakachi, T. Nishio, S. Mitusnaga, M. Ikeda, M. Konishi, S. Takahasi, N. Gotohda, S. Arahira, S. Zenda, T. Ogino, T. Kinoshita	Dose-volume histgram analysis of the safety of proton beam therapy for unresectable hepatocellular carcinoma	Int. J. Radiat. Oncol. Biol. Phys.	In press		2010
T. Nishio, A. Miyatake, T. Ogino, K. Nakagawa, N. Saijo, H. Esumi	The development and clinical use of a beam ON-LINE PET system mounted on a rotating gantry port in proton therapy	Int. J. Radiat. Oncol. Biol. Phys.	76(1)	277-286	2010
R. Kohno, E. Hirano, S. Kitou, T. Goka, K. Matsubara, S. Kameoka, T. Matsuura, T. Ariji, T. Nishio, M. Kawashima, T. Ogino	Evaluation of the usefulness of a MOSFET detector in an anthropomorphic phantom for 6-MV photon beam	Radiol. Phys. Technol.	3(2)	104-112	2010
S.Onodera, H.Aoyama, N. Katoh, H. Taguchi, K. Yasuda, D. Yoshida, K. Surtherland, R. Suzuki, M. Ishikawa, B. Gerard, S. Terasaka, H. Shirato	Long-term Outcomes of Fractionated Stereotactic Radiotherapy for Intracranial Skull Base Benign Meningiomas in Single Institution	Jpn J Clin Oncol	In press		2010
T. Inoue, N. Katoh, H. Aoyama, R. Onimaru, H. Taguchi, S. Onodera, S. Yamaguchi, H. Shirato	Clinical outcomes of stereotactic brain and/or body radiotherapy for patients with oligometastatic lesions	Jpn J Clin Oncol	In press		2010

T. Nishioka, M. Fujino, A. Homma, T. Yamashita, A. Sato, K. Ohmori, K. Obinata, H. Shirato, K. Notani, M. Nishio	Cesium implant for tongue carcinoma with a thickness of 1.5 cm or more: cases successfully treated with a Modified Manchester System	Yonsei Med J	51(4)	557-561	2010
K. Sutherland, S. Miyajima, H. Date, H. Shirato, M. Ishikawa, M. Murakami, M. Yamagiwa, P. Bolton, T. Tajima	A parameter study of pencil beam proton dose distributions for the treatment of ocular melanoma utilizing spot scanning	Radiol Phys Technol.	3(1)	16-22	2010
G. Bengua, M. Ishikawa, K. Sutherland, K. Horita, R. Yamazaki, K. Fujita, R. Onimaru, N. Katoh, T. Inoue, S. Onodera, H. Shirato	Evaluation of the effectiveness of the stereotactic body frame in reducing respiratory intrafractional organ motion using the real-time tumor-tracking radiotherapy system	Jpn. J. Med. Phys. Proc.	Int J Radiat Oncol Biol Phys.	630-636	2010
H. Onishi, H. Shirato, Y. Nagata, M. Hiraoka, M. Fujino, K. Gomi, K. Karasawa, K. Hayakawa, Y. Niibe, Y. Takai, T. Kimura, A. Takeda, A. Ouchi, M. Hareyama, M. Kokubo, T. Kozuka, T. Arimoto, R. Hara, J. Itami, T. Araki	Stereotactic Body Radiotherapy (SBRT) for Operable Stage I Non-Small-Cell Lung Cancer: Can SBRT Be Comparable to Surgery?	J Radiat Oncol Biol Phys.	In press		2010

M. Aristophanous, J. Rottmann, SJ. Park, S. Nishioka, H. Shirato, RI. Berbeco	Image-guided adaptive gating of lung cancer radiotherapy: a computer simulation study	Phys Med Biol.	55(15)	4321-4333	2010
RI. Berbeco, S. Nishioka, H. Shirato	Evaluation of the need for simultaneous orthogonal gated setup imaging	J Appl Clin Med Phys	11(2)	3203	2010
EW. Pepin, H. Wu, GA. Sandison, M. Langer, H. Shirato	Site-specific volumetric analysis of lung tumour motion	Phys Med Biol.	55(12)	3325-3337	2010
GR. Borst, M. Ishikawa, J. Nijkamp, M. Hauptmann, H. Shirato, G. Bengua, R. Onimaru, Bois A. de Josien, JV. Lebesque, JJ. Sonke	Radiation pneumonitis after hypofractionated radiotherapy: evaluation of the LQ(L) model and different dose parameters	Int J Radiat Oncol Biol Phys	77(5)	1596-1603	2010

書籍

著者氏名	論文タイトル名	書籍全体の編集者名	書　籍　名	出版社名	出版地	出版年	ページ
西尾禎治	粒子線治療の医学物理	大西洋、唐澤久美子、唐澤克之	がん放射線治療法２０１０	篠原出版新社	東京	2010	279-288

研究成果の刊行物・別刷

IOP PUBLISHING PHYSICS IN MEDICINE AND BIOLOGY

Phys. Med. Biol. **56** (2011) 965–977 doi:10.1088/0031-9155/56/4/006

A feasibility study of a molecular-based patient setup verification method using a parallel-plane PET system

Satoshi Yamaguchi[1], Masayori Ishikawa[1], Gerard Bengua[2], Kenneth Sutherland[1], Teiji Nishio[3], Satoshi Tanabe[1], Naoki Miyamoto[1], Ryusuke Suzuki[2] and Hiroki Shirato[4]

[1] Department of Medical Physics and Engineering, Hokkaido University Graduate School of Medicine, N-15 W-7 Kita-ku Sapporo 060-8638, Japan
[2] Department of Medical Physics, Hokkaido University Hospital, N-14 W-5 Kita-ku Sapporo 060-8648, Japan
[3] Particle Therapy Division, Research Center for Innovative Oncology, National Cancer Center, Kashiwa, 6-5-1 Kashiwano-ha, Kashiwa-shi, Chiba 277-8577, Japan
[4] Department of Radiology, Hokkaido University Graduate School of Medicine, N-15 W-7 Kita-ku Sapporo, 060-8638 Japan

E-mail: masayori@med.hokudai.ac.jp

Received 15 July 2010, in final form 9 December 2010
Published 19 January 2011
Online at stacks.iop.org/PMB/56/965

Abstract

A feasibility study of a novel PET-based molecular image guided radiation therapy (m-IGRT) system was conducted by comparing PET-based digitally reconstructed planar image (PDRI) registration with radiographic registration. We selected a pair of opposing parallel-plane PET systems for the practical implementation of this system. Planar images along the in-plane and cross-plane directions were reconstructed from the parallel-plane PET data. The in-plane and cross-plane FWHM of the profile of 2 mm diameter sources was approximately 1.8 and 8.1 mm, respectively. Therefore, only the reconstructed in-plane image from the parallel-plane PET data was used in the PDRI registration. In the image registration, five different sizes of ^{18}F cylindrical sources (diameter: 8, 12, 16, 24, 32 mm) were used to determine setup errors. The data acquisition times were 1, 3 and 5 min. Image registration was performed by five observers to determine the setup errors from PDRI registration and radiographic registration. The majority of the mean registration errors obtained from the PDRI registration were not significantly different from those obtained from the radiographic registration. Acquisition time did not appear to result in significant differences in the mean registration error. The mean registration error for the PDRI registration was found to be 0.93 $\pm$ 0.33 mm. This is not statistically different from the radiographic registration which had a mean registration error of 0.92 $\pm$ 0.27 mm. Our results suggest

that m-IGRT image registration using PET-based reconstructed planar images along the in-plane direction is feasible for clinical use if PDRI registration is performed at two orthogonal gantry angles.

(Some figures in this article are in colour only in the electronic version)

1. Introduction

Image guided radiotherapy (IGRT) techniques are presently used clinically to improve the accuracy of treatment delivery in photon radiation therapy. IGRT is used to correct for patient positioning errors prior to or during treatment by using image guided procedures. Patient setup can be verified through the co-registration of digitally reconstructed radiographs (DRR) and imaging plate (IP) or electronic portal imaging device (EPID) images taken using MV-x rays from a linear accelerator (Linac) while the patient is set up just prior to treatment (Dong and Boyer 1995, Gilhuijs *et al* 1996). Linac systems with on-board cone-beam computed tomography (CBCT) devices have also been developed (Pouliot *et al* 2005, Jaffray *et al* 2002, Groh *et al* 2002, Ford *et al* 2002, Munbodh *et al* 2006). CBCT allows the imaging of the target volume and organs at risk during treatment. Accuracy of patient setup verification error is important in order to ensure that the actual treatment geometry is as close as possible to the treatment planning geometry. At present, patient setup verification is done mostly by the alignment of bony structures in radiographic images taken during treatment and those used for treatment planning. The change in the tumor size and location inside the body is usually difficult to determine during treatment. Making the tumor visible in the irradiation field is thus desirable in order to improve setup verification accuracy.

Positron emission tomography (PET) based on sugar metabolism in the tumor caused by ^{18}F-fluorodeoxyglucose (FDG) uptake has been shown to be effective for distinguishing the tumor during diagnosis (Som *et al* 1980). Since PET images are functional images, they allow cell activity to be visible; thus, the tumor position can be determined. Another promising radioactive tracer for PET imaging is ^{18}F-fluoromisonidazole (FMISO) (Nehmeh *et al* 2008). FMISO is able to delineate hypoxic cells, which are known to be radiation resistant, in tumors. Clinical trials have demonstrated improved tumor control by delivering escalated doses to hypoxic tumor cells using IMRT and other techniques (Lee and Le 2008).

The spatial resolution and sensitivity of recent PET devices have also been significantly improved. This has been partly due to (1) the development of new detector elements such as BGO or GSO crystals, (2) the change in the acquisition method from 2D to 3D, and (3) the invention of depth-of-interaction (DOI) (Wienhard *et al* 2002, Yamaya *et al* 2003). The application of PET technology as a new modality for diagnostic procedures is also now being considered, for example, positron emission mammography (PEM) (Smith *et al* 2003, Huesman *et al* 2000, Zhang *et al* 2007, Raylman *et al* 2008, MacDonald *et al* 2009). In this study, we propose a PET-based molecular image guided radiation therapy (m-IGRT) system for patient setup verification in cases where significant tumor shrinkage or growth may occur, such as intracranial or head and neck. In the practical implementation of an m-IGRT system, it is preferable that the PET device is combined with a radiotherapy gantry to guarantee mechanical precision. There are, however, some restrictions on how the PET detectors can be mounted to the present gantry systems.

Because PET is a device that detects the annihilation radiation caused by positrons, it is necessary that at least a pair of opposed detectors are arranged to detect the two photons simultaneously. It is preferable that the isocenter of the pair of opposed detectors is identical to the isocenter of the radiotherapy unit. A structure with a wide open space between a pair of

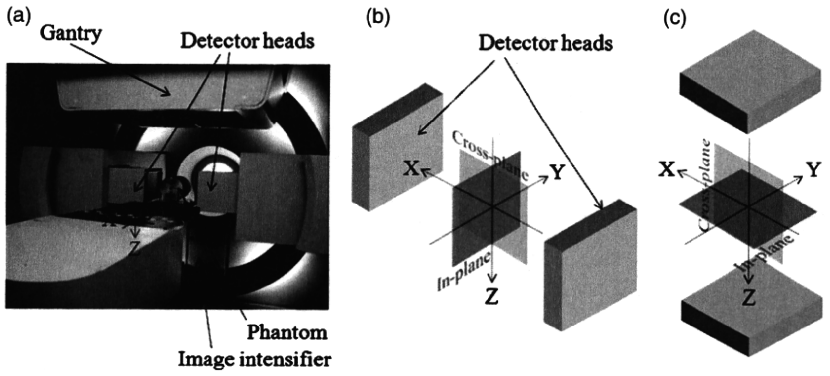

Figure 1. (a) The BOLPs with its gantry positioned at 0°. (b) The orientations of the in-plane and cross-plane directions in the BOLPs at a gantry angle of 0°. (c) The orientations of the in-plane and cross-plane directions in the BOLPs at a gantry angle of 90°.

opposed detectors is also needed so that the mega-voltage irradiation field does not become obstructed. The gantry rotation of the radiotherapy unit and the movement or the rotation of the couch must also be considered. Moreover, it is necessary to secure a wide field of view to use the device for setup verification. However, it is difficult in the conventional PET detector geometry, with ring-shape arrangement, to achieve this purpose. We therefore selected a geometry with a pair of opposing parallel-plane detectors. The advantage of this detector geometry is that it is structurally simple, and that it can be mounted easily on a radiotherapy gantry, similar to on-board imaging (OBI) devices.

In order to evaluate the feasibility of molecular image guided registration, we used the beam on-line PET system (BOLPs), developed at the Particle Therapy Division of the National Cancer Center, Kashiwa (Nishio *et al* 2005, 2006, 2010). The system consists of a pair of opposing parallel-plane detectors mounted on the gantry which can detect annihilation radiation produced by positron emitters (e.g. ^{15}O, ^{14}O, ^{13}N and ^{11}C). The BOLPs was originally developed for visualizing irradiation fields by measuring the activity of positron emitters which are generated by nuclear reactions from incident proton beams. The BOLPs has the same detector configuration as that of our proposed system.

In this paper, we report on the feasibility of a novel m-IGRT by comparing the PET-based digitally reconstructed planar image (PDRI) registration with radiographic registration.

2. Materials and method

2.1. Beam on-line PET system

The BOLPs at the National Cancer Center, Kashiwa, in Japan was used to verify the accuracy of patient setup verification in our proposed parallel-plane PET system. The BOLPs detector is mounted at the gantry of the proton irradiation system as shown in figure 1(a). The detector head consists of 3960 BGO crystals (2 mm × 2 mm × 20 mm) covering a 16 × 16 cm^2 field of view. The distance between the detector heads was fixed at 40 cm. Shown in figure 1(b) are the orientations of the in-plane and cross-plane directions for a gantry angle of 0°. The orientations of the in-plane and cross-plane directions for a gantry angle of 90° are illustrated in figure 1(c). The evaluation of the full width at half maximum (FWHM) of the profile of

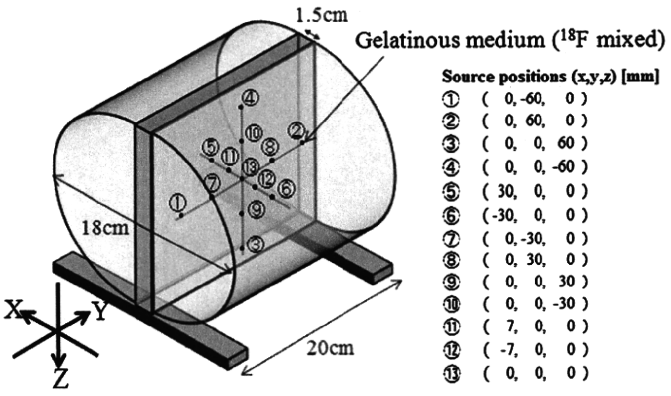

Figure 2. Cylindrical phantom with ^{18}F-sources placed in the positions as indicated.

2 mm diameter sources was done along the cross-plane and in-plane directions for a gantry angle of 0°. The FWHM of the profile is indicative of the spatial resolution.

In the image registration, only the reconstructed in-plane image from the parallel-plane PET data was used, and from here on, this in-plane image will be referred to as PDRI.

The BOLPs also includes an on-board x-ray system that allows the acquisition of radiographic images for patient setup verification. We compared the accuracy of radiographic and PDRI registrations.

2.2. Image reconstruction method

The detector configuration of the BOLPs is different from that of conventional PET systems in that they do not encircle the subject. Due to the parallel placement of the detector heads, there is limited angular sampling and loss of line of response (LOR) and the usual sinogram-based reconstruction method is not applicable. Therefore, the maximum likelihood-expectation maximization (MLEM) method (Shepp and Vardi 1982) was used in the LOR-based reconstruction using Siddon's algorithm (Siddon 1985).

In this study, only the detector sensitivity correction was applied while ignoring the other possible correction factors to account for scattering or absorption.

2.3. Phantom configuration

Two custom-made phantoms were used in our measurements. The first phantom was a polycarbonate cylindrical phantom with a width of 20 cm and a diameter of 18 cm. We refer to this phantom as the *cylindrical phantom*. It contained 13 cylindrical radiation sources (each with a diameter of 2 mm and width of 2 mm) that were arranged as shown in figure 2. The other phantom was a polycarbonate plate containing five cylindrical radiation sources of various diameters (i.e. 8, 12, 16, 24, 32 mm) with 1.5 cm width, representing different tumor sizes as shown in figure 3(a). This was attached to an acrylic slab (height: 20 cm, width: 18.5 cm, depth: 0.3 cm) as shown in figure 3(b). In this paper, we refer to this phantom setup as the *tumor phantom*. The radiation sources in both the cylindrical phantom and the tumor phantom used ^{18}F that was homogeneously mixed in a gelatinous medium.

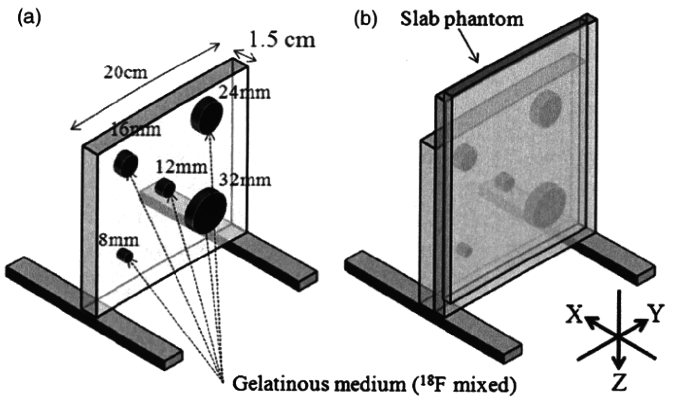

Figure 3. (a) Polycarbonate plate containing ^{18}F-sources of various diameters representing different tumor sizes. (b) The plate in (a) attached to an acrylic slab phantom.

2.4. FWHM of the profile of 2 mm diameter sources

The unique detector geometry of the BOLPs does not allow the use of the filtered back projection reconstruction as specified in the National Electrical Manufactures Association (NEMA) standard which is used for the evaluation of PET detectors. Therefore we used a modified method for image reconstruction based on PEM (Smith *et al* 2004, MacDonald *et al* 2009), which has a detector geometry similar to the BOLPs. PEM devices and the BOLPs have anisotropic spatial resolutions because the detectors do not encircle the object and do not rotate to acquire the full 360° angular sampling required for full three-dimensional tomography. Parallax error caused by the thickness of scintillation crystals is considered (Hoffman *et al* 1989, Lerche *et al* 2005).

We evaluated the FWHM of the profile of 13 cylindrical sources with a diameter of 2 mm and width of 2 mm using the cylindrical phantom shown in figure 2. The ^{18}F activity was 40 kBq ml^{-1}. The projection data were measured for 15 min at a gantry angle of 0°. The image reconstruction via the MLEM method was applied with the pixel size and slice thickness of 1.00 mm and a reconstruction volume of 15 × 15 × 15 cm^3.

2.5. Registration experiments

2.5.1. PDRI registration. PDRI registration was performed by comparing the in-plane digitally reconstructed planar image from the BOLPs and the image obtained from a conventional PET (Discovery ST, General Electric, Schenectady, New York). The pixel size and slice thickness were 3.91 and 3.27 mm, respectively. We placed the tumor phantom in a conventional PET such that the polycarbonate plate was parallel to the longitudinal axis and the center of the plate aligned with the isocenter. Data collection was performed for 15 min.

The tumor phantom was then placed at the isocenter of the BOLPs to obtain the data for the PDRI. Data were also collected for two additional conditions where the tumor phantom was displaced by 2 and 7 mm along the *Y*-axis, away from the isocenter to avoid the observer's bias from trial learning. Each measurement with the BOLPs was carried out for 5 min. The activity of ^{18}F was 20 kBq ml^{-1} and the background activity was 4 kBq ml^{-1}. The gantry angle was fixed at 0°. MLEM image reconstruction was applied with the pixel size and slice thickness of 1.00 mm and a reconstruction volume of 15 × 15 × 5 cm^3. PDRIs corresponding

to 1, 3 and 5 min measurements were generated for each setup position. Image registration based on the PDRI for each setup position was performed by five observers. The reference image was reconstructed from a conventional PET image.

2.5.2. Radiographic registration. To compare the accuracy of radiographic and PDRI registrations, we also performed image registration using images obtained from an x-ray CT and a fluoroscopic system. The tumor phantom was placed at the isocenter of the x-ray CT following the same setup as used in the PET measurement. The pixel size and slice thickness were 0.98 and 1.25 mm, respectively. Fluoroscope images of the tumor phantom were also taken using the installed fluoroscopic system in the proton irradiation system. The position of the tumor phantom was subsequently moved along the Y-axis to take additional data at 2 and 7 mm from the isocenter. The reference image used in the radiographic registration was the DRR reconstructed from x-ray CT.

2.5.3. Registration accuracy evaluation. To evaluate the accuracy of the registration methods, image registration trials using in-house software were performed for ten trials. Each trial consisted of five different images shown twice to the observers. Five observers estimated the shifts in each trial. From the image registration data, we calculated the registration error (RE) using equation (1). Actual shift (Y_{actual}) was 0, 2 and 7 mm along the Y-axis. Z_{obs} and Y_{obs} in the equation refer to the observed translation along the Z-axis and Y-axis respectively performed by the five subjects. Statistical analysis was performed based on the registration error for both the radiographic and PDRI registrations:

$$\text{RE(mm)} = \sqrt{(Z_{\text{obs}})^2 + (Y_{\text{obs}} - Y_{\text{actual}})^2}. \tag{1}$$

Here RE denotes the registration error, Z_{obs} the observed translation along the Z-axis, Y_{obs} the observed translation along the Y-axis and Y_{actual} the actual setup couch translation along the Y-axis (0, 2, 7 mm).

2.5.4. Statistical analysis. Statistical analysis of our data was performed using JMP 8 (SAS Institute Inc.) software. The mean registration error and standard deviation (SD) for the various diameters were determined based on the acquisition time for data collection (i.e. 1, 3 and 5 min) and modality (BOLPs, x-ray fluoroscopy). Data were analyzed by one-way ANOVA, while the differences among means were analyzed by two-sided Student's t-test with the level of statistical significance set to $p < 0.05$.

3. Results

3.1. FWHM of the profile of 2 mm diameter sources

Figure 4 shows the reconstructed in-plane and cross-plane images of the cylindrical phantom corresponding to a gantry angle of 0°. The reconstructed source diameter at the central position was larger than the others due to blurring caused by adjacent sources. The FWHM of each radiation source is shown in figure 5. The mean ± SD for FWHM was 1.8 ± 0.3 mm in the in-plane image and 8.1 ± 1.2 mm in the cross-plane image at a gantry angle of 0°.

3.2. Registration accuracy evaluation

Shown in figure 6 are the PDRIs of the tumor phantom at a gantry angle of 0°. Images from left to right correspond to the three acquisition times (1, 3 and 5 min) for data collection,

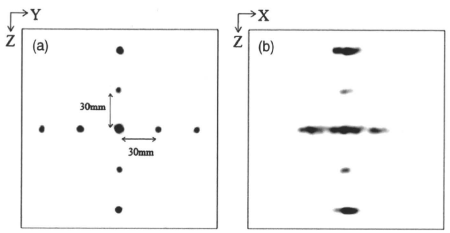

Figure 4. Planar images of the ^{18}F-sources along the (a) in-plane and (b) cross-plane directions reconstructed from the BOLPs data at a gantry angle of 0°.

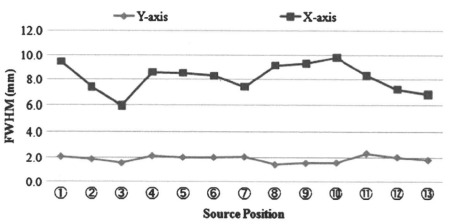

Figure 5. FWHM of the profile of the 2 mm diameter sources in the cylindrical phantom of figure 2.

while those from top to bottom correspond to the positions of the phantom (0, 2 and 7 mm) during data acquisition. The gray-scale window level of the images was adjusted to enhance the contrast. The measured activity at the source increased linearly as a function of acquisition time, and contrast to the background was constant and no inconsistency was observed among the three positions.

Figure 7 shows the variations in the observed PDRI and radiographic registration errors with respect to the acquisition time, phantom position and source diameter. PDRI registration errors were obtained from the registration of the reconstructed PET and BOLPs planar images. The radiographic registration errors were obtained from registration of DRR and portal (x-ray) images. The dependence of the registration error on the phantom position was not seen for each diameter.

Shown in table 1 are the mean ± SD of the registration errors based on our ANOVA. For the diameter of 8 mm the mean registration error of the PDRI registration appears to be influenced by the acquisition time with the longest acquisition time having the least mean registration error. The registration error for the radiographic registration was comparable to that of the shortest acquisition time of 1 min for the PDRI. The differences in the registration error between the image registration modalities listed in table 1 for the 8 mm diameter were found to be significant at a p-value of <0.0001. On the other hand, the mean registration error in all four registration methods for the diameter of 12 mm was found to be statistically insignificant ($p = 0.3545$) with their mean registration error ranging between 0.49 and 0.63. For diameters of 16 and 24 mm, the three acquisition times using the PDRI resulted in similar

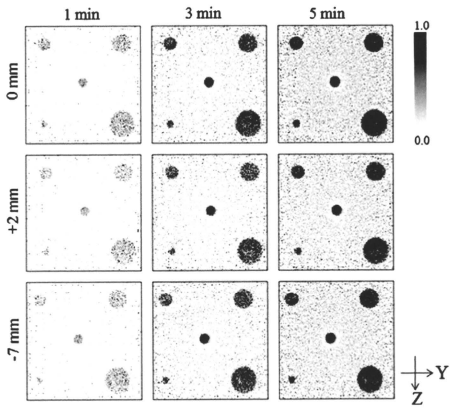

Figure 6. Planar image reconstructions of the ^{18}F-sources in the tumor phantom of figure 3(b). Shown are the results for three phantom positions relative to the isocenter and at the acquisition times of 1 , 3 and 5 min, respectively.

Table 1. Statistical comparison of registration errors from PDRI and radiographic registrations using ANOVA. PDRI registration was performed using reconstructed planar images from PET data (at the acquisition time of 15 min) and BOLPs data (at the acquisition times of 1, 3 and 5 min). Radiographic registration was performed using DRR and portal (x-ray) images.

	Diameter				
Registration method	8 mm	12 mm	16 mm	25 mm	32 mm
PDRI (1 min)	1.07 ± 0.42	0.49 ± 0.34	1.02 ± 0.44	1.28 ± 0.35	1.12 ± 0.39
PDRI (3 min)	0.87 ± 0.29	0.59 ± 0.24	1.01 ± 0.38	1.25 ± 0.29	0.86 ± 0.37
PDRI (5 min)	0.56 ± 0.26	0.60 ± 0.24	1.00 ± 0.34	1.30 ± 0.26	0.88 ± 0.32
Radiographic (x-ray)	0.98 ± 0.28	0.63 ± 0.30	0.87 ± 0.31	0.95 ± 0.20	1.17 ± 0.26
p-value	<0.0001*	0.3545	0.522	0.0003*	0.0044*

*Significant ($p < 0.05$).

registration errors and a relatively smaller registration error for the radiographic registration. However, the difference between the PDRI and radiographic registrations was found to be statistically significant only for 24 mm at $p = 0.0003$. A significant difference between the PDRI and radiographic registration errors was obtained for the 32 mm diameter.

The statistical comparisons of the mean registration error and SD for each source diameter obtained from the PDRI registration at 1, 3, and 5 min and the radiographic registration are shown in figures 8 and 9.

For the diameter of 8 mm, the differences in the registration error for the three acquisition times used in the PDRI registration were found to be statistically significant. However, when compared to the registration error of the radiographic registration, only the 5 min PDRI data yielded a significant difference. The mean registration errors for the image registration

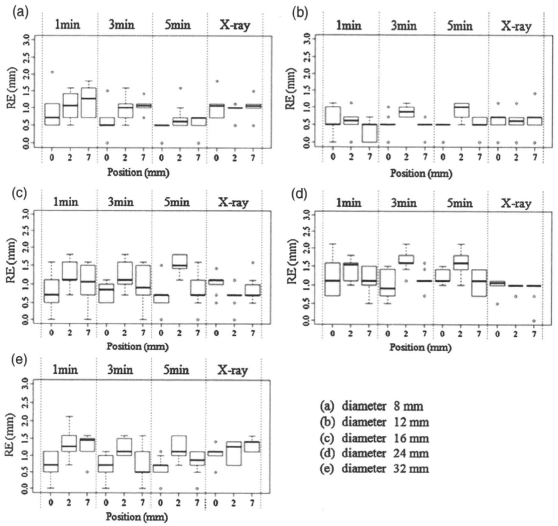

Figure 7. Registration errors for the tumor phantom of figure 3(b). Shown are the results for three phantom positions relative to the isocenter (0), isocenter + 2 mm (2) and isocenter + 7 mm (7) at the acquisition times of 1 , 3 and 5 min, respectively.

conditions shown in figures 8(b) and (c) for diameters of 12 and 16 mm were not statistically different. However, a larger variation in the computed registration error was observed for 16 mm.

For the diameter of 24 mm, the mean registration error obtained for the radiographic registration was found to be significantly smaller compared to those obtained using the PDRI registration method. Furthermore, the acquisition time did not appear to result in significant differences in the mean registration error for the PDRI registration. Like those of the results for the 8 mm diameter, the mean registration error for the 32 mm diameter decreased with the acquisition time in the PDRI registration.

A comparison of the registration error SDs is shown in figure 9 for the various diameters and data acquisition methods. The SDs for most of the results were not statistically different. The image registration SDs of the PDRI at 3 min acquisition time were statistically the same as those of the radiographic registration.

4. Discussion

An overall evaluation of the accuracy of PDRI registration independent of the source size is necessary. We therefore performed a comparative study of the registration error obtained with PDRI and radiographic registrations for a number of hypothetical source sizes. The cumulative

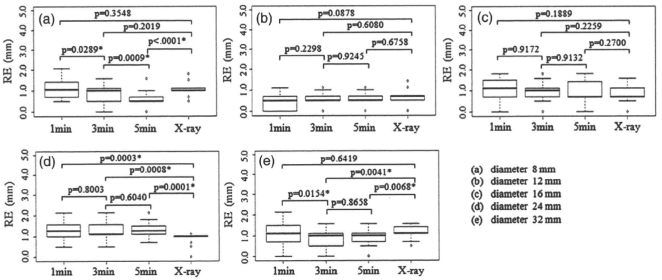

Figure 8. Statistical comparison of the mean registration error for the five cylindrical sources with diameters of 8, 12, 16, 24 and 32 mm using Student's *t*-test at $p < 0.05$ significance level.

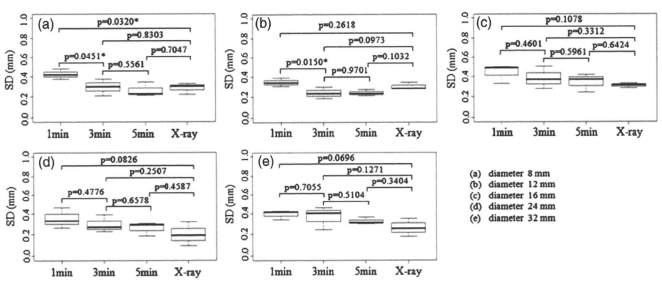

Figure 9. Statistical comparison of the standard deviation of the mean registration error for the five cylindrical sources with diameters of 8, 12, 16, 24 and 32 mm using Student's *t*-test at $p < 0.05$ significance level.

mean registration error and SD for five different source sizes using four registration conditions (i.e. PDRI at 1, 3 and 5 min acquisition times and radiographic registration) are shown in figure 10. A general trend of decreasing mean registration error and SD for longer acquisition time is seen for the PDRI registration. The 3 min data acquisition in the BOLPs yielded comparable results to radiographic registration, while the 5 min acquisition appears to result in lower registration error.

Our tumor phantom experiments show that the mean of the registration errors for the PDRI is approximately 0.93 mm and the SD is approximately 0.33 mm. This is not statistically different from the radiographic registration which had a mean registration error of 0.92 $\pm$ 0.27 mm.

Although there are no reports on the accuracy of image registration using molecular imaging, there have been a number of publications regarding the accuracy of DRR and EPID image registration. Dong and Boyer (1995) showed that in their phantom image registration study, the correlation procedure had a SD of 0.5 mm in aligning translational shifts. Gilhuijs

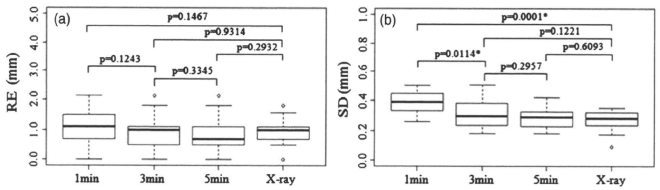

Figure 10. Statistical comparison of (a) the mean registration error and (b) the standard deviation for an overall evaluation using Student's t-test at $p < 0.05$ significance level.

et al (1996) registered 2D portal images with CT data, and their automatic 3D analysis of patient setup accuracy was found to be accurate to within 1 mm in the translational directions. In the clinical evaluation of patient setup errors using portal imaging by Hurkmans *et al* (2001), it was reported that setup errors were less than 2.0 mm (1SD) for head and neck, 2.5 mm (1 SD) for prostate, 3.0 mm (1 SD) for general pelvic and 3.5 mm (1 SD) for lung cancer. The study also noted that the setup verification accuracy varies widely, depending on the treatment site, method of immobilization and institution.

The registration error for the PDRI was lower than that of previously reported radiographic registrations. This could be due to the fact that the image registration was performed with ^{18}F-source itself, not with the skeletal structure, or that there was a phantom dependence. Nevertheless, the registration error for PDRI registration was not significantly different from that of radiographic registration in our experiments. As shown in figure 10(b), the registration error is dependent on the data acquisition time. In order to apply PDRI registration clinically, the acquisition time should be taken into account. A longer acquisition time will result in lower registration error, but it will cause patient discomfort. An optimum acquisition time needs to be considered while maintaining the registration accuracy. However, this is complicated because it depends on the tumor and normal tissue uptake and radiation attenuation in the patient's body. Patient immobilization may also be necessary in order to minimize the effects of inter- and intra-fraction motion caused by patient movement. The effect of respiratory induced motion should be considered in future works.

If FDG is used as the tracer in PDRI registration, it will also be taken up in normal organs such as the brain, liver, kidneys, bladder, etc. This will be a problem in this image registration modality. However, because of the high spatial resolution of our parallel-plane PET system along the in-plane direction, it should be possible to distinguish the tumor FDG uptake from that of the adjacent normal organs which also accumulate FDG. As shown in Figure 4, at the same gantry angle, the corresponding cross-plane image has a much lower resolution and therefore would not be usable for image registration.

Conventional radiographic registration is performed by taking a portal planar image in the LR direction with the gantry at 0° and afterward rotating the gantry to 90° in order to take another portal planar image at the AP direction. These left–right (LR) and anterior–posterior (AP) images are separately registered with corresponding DRR images to complete the radiographic registration process. In our m-IGRT system, the same setup verification procedure using LR and AP images taken separately at different gantry angles will have to be performed. In this case, the PDRI for the LR direction will be the reconstructed in-plane image from the parallel-plane PET data obtained at a gantry angle of 0°. On the other hand, the PDRI for the AP direction will be the reconstructed in-plane image from parallel-plane

PET data obtained at a gantry angle of 90°. The measurement time for each gantry angle is expected to be only a few minutes; therefore, the effects on the acquired parallel-plane PET data of metabolic changes in the body or source activity are negligible.

Additionally, this high spatial resolution will likewise be useful in hypoxic region imaging using FMISO because the hypoxic region distribution in the tumor is complex (Nehmeh *et al* 2008).

5. Conclusion

We performed a basic study to determine the accuracy of image registration using a PET-based molecular image guided method. Planar images were reconstructed from parallel-plane PET data to obtain the PET-based digitally reconstructed planar image (PDRI) used in the registration. In-plane PDRIs had higher resolution and therefore usable for image registration. Phantom experiments using in-plane PDRIs showed that there is no significant difference between radiographic and PDRI registrations. Our results suggest that m-IGRT image registration using PET-based reconstructed planar images along the in-plane direction is feasible for clinical use. Furthermore, the system will provide additional information for image registration when bony structures cannot be recognized with radiographic registration methods.

Acknowledgments

This research was a part of the 'Innovation COE Program for Future Drug Discovery and Medical Care' project and partially supported by the Grant-in-Aid for Special Coordination Funds for Promoting Science and Technology of the Japanese Ministry of Education, Culture, Sports, Science and Technology. The authors are also grateful to the assistance given by the Proton Radiotherapy Department of the National Cancer Center, Kashiwa staff during the experiments with the BOLPs. This research was partially supported by Health and Labour Science Research Grants from the Japanese Government.

References

Dong L and Boyer A L 1995 An image correlation procedure for digitally reconstructed radiographs and electronic portal images *Int. J. Radiat. Oncol. Biol. Phys.* **33** 1053–60

Ford E C, Chang J, Mueller K, Sidhu K, Todor D, Mageras G, Yorke E, Ling C C and Amols H 2002 Cone-beam CT with megavoltage beams and an amorphous silicon electronic portal imaging device: potential for verification of radiotherapy of lung cancer *Med. Phys.* **29** 2913–24

Gilhuijs K G A, van de Ven P J H and van Herk M 1996 Automatic three-dimensional inspection of patient setup in radiation therapy using portal images, simulator images, and computed tomography data *Med. Phys.* **23** 389–99

Groh B A, Siewerdsen J H, Drake D G, Wong J W and Jaffray D A 2002 A performance comparison of flat-panel imager-based MV and kV cone-beam CT *Med. Phys.* **29** 967–75

Hoffman E J *et al* 1989 PET system calibrations and corrections for quantitative and spatially accurate images *IEEE Trans. Nucl. Sci.* **36** 1108–12

Huesman R H *et al* 2000 List-mode maximum-likelihood reconstruction applied to positron emission mammography (PEM) with irregular sampling *IEEE Trans. Med. Imaging* **19** 532–7

Hurkmans C W *et al* 2001 Set-up verification using portal imaging: review of current clinical practice *Radiother. Oncol.* **58** 105–20

Jaffray D A, Siewerdsen J H, Wong J W and Martinez A A 2002 Flat-panel cone-beam computed tomography for image-guided radiation therapy *Int. J. Radiat. Oncol. Biol. Phys.* **53** 1337–49

Lee N Y and Le Q T 2008 New developments in radiation therapy for head and neck cancer: intensity-modulated radiation therapy and hypoxia targeting *Semin. Oncol.* **35** 236–50

Lerche C W *et al* 2005 Depth of γ-ray interaction within continuous crystals from the width of its scintillation light-distribution *IEEE Trans. Nucl. Sci.* **52** 560–72

MacDonald L *et al* 2009 Clinical imaging characteristics of the positron emission mammography camera: PEM Flex Solo II *J. Nucl. Med.* **50** 1666–75

Munbodh R, Jaffray D A, Moseley D J, Chen Z, Knisely J P S, Cathier P and Duncan J S 2006 Automated 2D–3D registration of a radiograph and a cone beam CT using line-segment enhancement *Med. Phys.* **33** 1398–411

Nehmeh S A *et al* 2008 Reproducibility of intratumor distribution of ^{18}F-fluoromisonidazole in head and neck cancer *Int. J. Radiat. Oncol. Biol. Phys.* **70** 235–42

Nishio T *et al* 2005 Distributions of β+ decayed nuclei generated in the CH_2 and H_2O targets by the target nuclear fragment reaction using therapeutic MONO and SOBP proton beam *Med. Phys.* **32** 1070–82

Nishio T *et al* 2006 Dose-volume delivery guided proton therapy using beam online PET system *Med. Phys.* **33** 4190–7

Nishio T *et al* 2010 The development and clinical use of a beam on-line PET system mounted on a rotating gantry port in proton therapy *Int. J. Radiat. Oncol. Biol.Phys.* **76** 277–86

Pouliot J *et al* 2005 Low-dose megavoltage cone-beam CT for radiation therapy *Int. J. Radiat. Oncol. Biol. Phys.* **61** 552–60

Raylman R R *et al* 2008 The positron emission mammography/tomography breast imaging and biopsy system (PEM/PET): design, construction and phantom-based measurements *Phys. Med. Biol.* **53** 637–53

Shepp L A and Vardi Y 1982 Maximum likelihood reconstruction for emission tomography *IEEE Trans. Med. Imaging.* **1** 113–22

Siddon R L 1985 Fast calculation of the exact radiological path for a three dimensional CT array *Med. Phys.* **12** 252–5

Smith M F *et al* 2003 Analysis of factors affecting positron emission mammography (PEM) image formation *IEEE Trans. Nucl. Sci.* **50** 53–9

Smith M F *et al* 2004 Positron emission mammography with tomographic acquisition using dual planar detectors: initial evaluations *Phys. Med. Biol.* **49** 2437–52

Som P *et al* 1980 A fluorinated glucose analog, 2-fluoro-2-deoxy-D-glucose (F-18): nontoxic tracer for rapid tumor detection *J. Nucl. Med.* **21** 670–5

Wienhard K *et al* 2002 The ECAT HRRT: performance and first clinical application of the new high resolution research tomograph *IEEE Trans. Nucl. Sci.* **49** 104–10

Yamaya T, Hagiwara N, Obi T, Yamaguchi M, Kita K, Ohyama N, Kitamura K, Hasegawa T, Haneishi H and Murayama H 2003 DOI-PET image reconstruction with accurate system modeling that reduces redundancy of the imaging system *IEEE Trans. Nucl. Sci.* **50** 1404–9

Zhang J *et al* 2007 Study of the performance of a novel 1 mm resolution dual-panel PET camera design dedicated to breast cancer imaging using Monte Carlo simulation *Med. Phys.* **34** 689–702

Diseases of the Esophagus (2010) **, **–**
DOI: 10.1111/j.1442-2050.2010.01141.x

DISEASES OF THE ESOPHAGUS

Original article

Submucosal tumor appearance is a useful endoscopic predictor of early primary-site recurrence after definitive chemoradiotherapy for esophageal squamous cell carcinoma

C.-H. Tu,[1] M. Muto,[2] T. Horimatsu,[2] K. Taku,[3] T. Yano,[4] K. Minashi,[4] M. Onozawa,[5] K. Nihei,[5] S. Ishikura,[5] A. Ohtsu,[4] S. Yoshida[4]

[1]*Division of Gastroenterology and Hepatology, Department of Internal Medicine, Far Eastern Memorial Hospital, Taipei, Taiwan; and* [2]*Department of Gastroenterology and Hepatology, Kyoto University, Kyoto, Japan, and* [3]*Division of Gastrointestinal Oncology, Shizuoka Cancer Center, Shizuoka, Japan,* [4]*Division of Digestive Endoscopy and Gastrointestinal Oncology, National Cancer Center Hospital East, Kashiwa, Japan, and* [5]*Division of Radiation Oncology, National Cancer Center Hospital East, Kashiwa, Japan*

SUMMARY. **Chemoradiotherapy (CRT) for esophageal cancer is disadvantageous because of a high locoregional failure rate. Detecting early small recurrent cancers at the primary site is necessary for potential salvage treatment. However, most endoscopists are inexperienced and therefore, a role for surveillance endoscopy after complete remission (CR) has not been established. We retrospectively evaluated serial surveillance endoscopic images from patients eventually proved to have primary-site recurrence in order to identify useful endoscopic features for early diagnosis. From January 2000 to December 2004, 303 patients with esophageal squamous cell carcinoma underwent definitive CRT, and 133 of them achieved CR. The surveillance endoscopic images stored at intervals of 1–3 months for the 16 patients with recurrence only at the primary tumor site and the 61 patients with no recurrence were collected for reexamination. Among 133 patients who achieved CR, 16 (12%) developed only local recurrence at the primary site. Thirteen of the 16 primary-site recurrent tumors (81%) appeared as submucosal tumors (SMT), with the remaining appearing as erosions or mild strictures. Of biopsy-proven recurrences, 81% were preceded by newly developed lesions such as SMT, erosions, or mild strictures detected by earlier surveillance endoscopies. For all 77 patients achieving CR with no metastasis, 86% of the evolving SMT with negative biopsies were eventually confirmed as cancer at later endoscopies. Thirteen of the 21 evolving lesions were subsequently confirmed as recurrent cancer. Early primary-site recurrence of esophageal cancer after a complete response to CRT is detectable with frequent endoscopic surveillance. SMT appearance is a useful endoscopic sign of early recurrence, as well as a predictor of subsequent diagnosis of recurrence.**

KEY WORDS: **chemoradiotherapy, esophageal cancer, recurrence, surveillance.**

INTRODUCTION

Definitive chemoradiotherapy (CRT) is widely accepted as a standard treatment option in the management of locally advanced esophageal cancer because of its high response rate and significant survival benefit.[1,2] A major drawback to this nonsurgical approach is locoregional treatment failure. At least 40% of patients undergoing CRT experienced local failure, some of whom did not develop distant metastases.[1,3–5]

These primary-site recurrence patients are traditionally managed with salvage esophagectomy for a chance of long-term survival, particularly in those with an earlier pathological stage (T1N0 and T2N0).[6,7] However, high perisurgical mortality and morbidity rates are major concerns.[7,8] Recently developed nonsurgical techniques, such as salvage endoscopic mucosal resection and photodynamic therapy,

Address correspondence to: Dr Manabu Muto, MD PhD, Department of Gastroenterology and Hepatology, Kyoto University, 54 Kawaharacho, Shogoin, Sakyo-ku, Kyoto 606-8507, Japan. Email: mmuto@kuhp.kyoto-u.ac.jp
List of presentations: Nil.
Author's disclosure of potential conflict of interest: The authors have no potential conflicts of interest.

have the advantages of greater safety and fewer treatment-related sequelae, while conferring promising survival benefits for local failures after definitive CRT.[9,10] Technically, endoscopic mucosal resection and photodynamic therapy are feasible only when the volume of the locally recurrent tumor is small enough to be amenable to these endoscopy-based procedures. Therefore, the application of these newer treatments depends crucially on the ability to identify early recurrent tumors by endoscopy.

A strategy of frequent surveillance endoscopy initiated early after remission of the cancer should theoretically improve the chances of detecting primary-site recurrent tumors in their early stages. This requires the prompt recognition of minute tumors arising from the former neoplastic bed, instead of from the uninvolved normal esophageal mucosa. However, the complete regression of cancer cells results in residual fibrosis, radiation-induced tissue injury, and the distortion of normal microstructures,[11,12] which may render relapsing neoplastic growth morphologically different from typical primary tumors. Apparently, most endoscopists are inexperienced in hunting for these difficult lesions. To our knowledge, no study of the skills in endoscopic detection of such lesions has been published. Not surprisingly, a follow-up endoscopy after the completion of CRT is considered 'optional' in the National Comprehensive Cancer Network clinical practice guidelines for esophageal cancer.[13] We believe that a reliable endoscopic diagnostic technique is necessary to support a strategy of intense endoscopic follow-ups.

As a cancer referral and research hospital, our institute is unique in its implementation of a vigorous endoscopic follow-up program after primary treatment for all patients with esophageal cancer. Therefore, it is possible to analyze the filed imaging data of endoscopic monitoring on the post-CRT mucosa. In the present study, we aimed to identify useful endoscopic findings through reviewing the image data pool to predict recurrent esophageal cancers limited to the primary site after complete remission (CR) is achieved by CRT.

MATERIALS AND METHODS

Patient population

Between January 2000 and December 2004, 303 patients with esophageal squamous cell carcinoma underwent definitive CRT at the National Cancer Center Hospital East, Kashiwa, Japan. The CRT consisted of 50.4–60 Gy irradiation, together with two cycles of continuous infusion with 5-fluorouracil (5FU) and cisplatin. Up to four courses of CRT were added for those patients who showed a good initial response to treatment.[9]

Table 1 Clinical data of 133 patients achieving complete remission with definitive chemoradiotherapy

Characteristic		Number of patients	%
Sex			
Male		110	82.7
Female		23	17.3
Age (years)			
Mean	62		
Range	39–76		
T stage			
T1		30	22.6
T2		21	15.8
T3		70	52.6
T4		12	9.0
N stage			
N0		46	34.6
N1		87	65.4
M stage			
M0		123	92.5
M1		10	7.5
Clinical stage			
I		16	12.0
II		45	33.8
III		62	46.6
IV		10	7.5
Macroscopic classification			
Type 0		30	22.6
Type 1		19	14.3
Type 2		60	45.1
Type 3		24	18.0

Response to treatment was assessed at the completion of CRT. CR was defined when all the following criteria were met: (i) the disappearance of the tumor lesion or ulcer at the primary site, with negative biopsies; (ii) no esophageal stricture or any condition that prevented a thorough endoscopic examination of the whole esophagus; (iii) no remaining measurable disease or distant metastasis on computer tomography and chest roentgenography; and (5) these criteria were met for at least 4 weeks.

Of the 303 patients, 133 (43.9%) were defined as being in CR at the completion of CRT. Of these 133 patients, 110 were men, with a median age of 62 years. Pretreatment staging of their esophageal cancers was determined with the tumor-node-metastasis classification of the International Union Against Cancer.[14] Seventy (52.6%) patients had T3 tumors; most patients had N1 (65.4%) or M0 (92.5%) disease. Forty-five (33.8%) and 62 (46.6%) patients were classified as clinical stages II and III, respectively (Table 1).

Study design

After achieving CR, initial follow-up endoscopy to confirm CR was scheduled within at most 1–2 months for each patient, accompanied with other necessary studies for the assessment of metastases. After the confirmation of CR, follow-up endoscopy was scheduled every 2–3 months for the first year and every 4–6